

# HisTrackMap: Global Vectorized High-Definition Map Construction via History Map Tracking

Jing Yang<sup>\* †</sup>  
Tongji University

Sen Yang<sup>\*</sup>  
Baidu Inc.

Xiao Tan  
Baidu Inc.

Hanli Wang<sup>‡</sup>  
Tongji University

## Abstract

As an essential component of autonomous driving systems, high-definition (HD) maps provide rich and precise environmental information for auto-driving scenarios; however, existing methods, which primarily rely on query-based detection frameworks to directly model map elements or implicitly propagate queries over time, often struggle to maintain consistent temporal perception outcomes. These inconsistencies pose significant challenges to the stability and reliability of real-world autonomous driving and map data collection systems. To address this limitation, we propose a novel end-to-end tracking framework for global map construction by temporally tracking map elements' historical trajectories. Firstly, instance-level historical rasterization map representation is designed to explicitly store previous perception results, which can control and maintain different global instances' history information in a fine-grained way. Secondly, we introduce a Map-Trajectory Prior Fusion module within this tracking framework, leveraging historical priors for tracked instances to improve temporal smoothness and continuity. Thirdly, we propose a global perspective metric to evaluate the quality of temporal geometry construction in HD maps, filling the gap in current metrics for assessing global geometric perception results. Substantial experiments on the nuScenes and Argoverse2 datasets demonstrate that the proposed method outperforms state-of-the-art (SOTA) methods in both single-frame and temporal metrics. The project page is available at: <https://yj772881654.github.io/HisTrackMap>.

## 1. Introduction

High-definition (HD) maps, which include vectorized map elements such as lane dividers, pedestrian crossings, and road boundaries, play a critical role in the navigation and

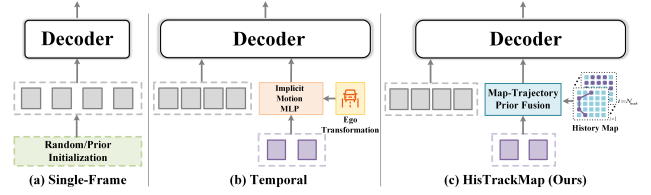


Figure 1. **Comparison of Different HD Map construction Paradigms.** (a) Single-Frame, (b) Temporal, (c) HisTrackMap (Ours). The gray square represents detect queries, while the purple square represents temporal propagation queries.

planning of autonomous driving [11, 23, 31–33]. Traditional map construction methods use the SLAM-based method [25, 26, 40] to collect offline map data, followed by extensive post-processing to generate HD maps. However, these methods are constrained by significant limitations, including substantial costs, the absence of real-time processing capabilities, and difficulties in accommodating dynamic environments and road updates.

Recent advancements in Perspective View (PV)-to-Bird’s-Eye View (BEV) methods have significantly enhanced vectorized HD map construction such as [7, 10, 13, 14]. These approaches leverage the DETR-based detection paradigm [2] to achieve precise HD map generation. To illustrate the differences across various paradigms, we present a comparison in Fig.1. Specifically, Fig.1 (a) showcases the single-frame architecture, which directly generates vectorized maps by decoding parallel learnable or prior-initialized queries using a decoder to interact with BEV feature. Nevertheless, internal prediction instabilities within the model coupled with uncontrollable environmental factors, such as occlusions or low-light conditions, frequently result in temporal perception inconsistencies, posing substantial challenges for real-world autonomous driving scenarios. Fig.1 (b) describes the temporal architecture, where latent query embedding is used as a stream memory [29, 37], facilitating the propagation of temporal information within a unified latent memory. Furthermore, MapTracker [3] employs a tracking paradigm that further utilizes query propagation and implicit latent memory to

<sup>\*</sup>Equal contribution.

<sup>†</sup>Work done during an internship at Baidu.

<sup>‡</sup>Corresponding authors.

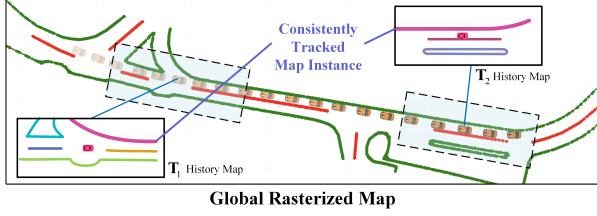


Figure 2. **The global rasterized map with history maps.** Red and green represent divider and boundary categories, respectively. In the history maps, different colors indicate unique tracked map instances. The pink instance is tracked at  $T_1$ , consistently propagating temporal geometric information and providing priors for the corresponding track query at  $T_2$ .

associate instance-level map elements across consecutive frames, enhancing temporal consistency. In such a framework, a Motion MLP proposed in [37] is essential for obtaining the next-frame latent memory considering the pose transformation between consecutive frames. Consequently, it employs a transformation loss to guide the Motion MLP, implicitly ensuring the accuracy of the pose transformation.

It is understood that a substantial amount of historical perception map data generated during vehicle navigation could potentially be leveraged as prior knowledge or utilized to reduce computational overhead in overlapping map regions. However, the current approach of implicit encoding through instance queries remains inadequate for precisely recording or preserving past geometric map information. To fully utilize existing perception results, as shown in Fig. 1 (c), we propose HisTrackMap, which explicitly maintains instance-level history maps for corresponding map instances under a tracking paradigm. This approach provides prior information for subsequent navigation perception, ensuring smoother and more continuous HD map construction and enhancing the efficiency and accuracy of temporal information propagation. Fig. 2 illustrates the global rasterized map generated from a continuous navigation sequence, along with details of instance tracking. Furthermore, we propose Map-Trajectory Prior Fusion, which leverages the history map to provide refined prior information for track queries at the subsequent timestamp by integrating position-aligned PV and BEV features. Our HisTrackMap leverages instance-level history maps to establish one-to-one correspondences between track queries and map trajectories, thereby enhancing global geometric consistency and constructing a temporally consistent vectorized HD map.

Although traditional Chamfer Distance mean Average Precision (mAP) metrics are widely used for HD map construction, we argue that single-frame metrics are insufficient for evaluating performance in practical autopilot scenarios and map data collection processes. For example, they fail to maintain global constructed map consistency across sequential frames, which is critical to ensure robust long-term perception, reliable decision-making, and efficient data ac-

quisition. While MapTracker introduced consistency-aware metrics (C-mAP) to penalize inconsistent map elements, they remain indirect methods of evaluation. To address this issue, we propose a global geometric-aware metric (G-mAP), which directly evaluates the global perceptual quality of the entire scene. The proposed HisTrackMap consistently outperforms existing methods, demonstrating the effectiveness of utilizing history maps compared to implicit transformations.

In summary, our main contributions are as follows:

- An end-to-end tracking-enhanced framework, HisTrackMap, for vectorized HD map construction is proposed, which leverages temporal information by maintaining instance-level history maps, reducing redundant computations, and enhancing efficiency.
- The Map-Trajectory Prior Fusion module is designed to fully utilize the map trajectory information from the history map, combined with instance-level perception features, to provide priors for the corresponding track queries in future frames, thereby optimizing the temporal propagation process.
- A novel benchmark with a global geometric perspective is introduced to address the limitations of existing evaluation methods in practical applications. Our HisTrackMap achieves SOTA results in the popular nuScenes [1] and Argoverse 2 [30] datasets.

## 2. Related Work

**Map Perception with Single Frame.** Recently, with advances in PV-to-BEV methods [12, 18–20, 22, 34], the HD map construction has predominantly been formulated as a detection task using surround-view images from vehicle-mounted cameras in a single-frame setting. MapTR [13, 14] proposes a unified approach for map elements, addressing ambiguities and ensuring stable learning. In representing map elements, PivotNet [5] adopts a pivot-based representation, while GeMap [42] models geometric features through Euclidean shapes. MGMapNet [35] leverages multi-granularity representations to model map instances, integrating instance-level and point-level queries.

**Map Perception with Priors.** Some of the latest methods have also focused on integrating rasterized results and standard (SD) maps to provide priors for HD map construction. SMERF [21] integrates SD maps for online map prediction, with PMapNet [9] enhancing performance by focusing on relevant SD Map skeletons. TopoSD [36] encodes SD map elements into neural representations and instance tokens, using them as priors for lane geometry and topology decoding. Mask2Map [4] uses a two-stage framework, generating a rasterized map via a segmentation network and refining it into a vectorized map with a mask-driven network. HRMapNet [41] leverages historical rasterized maps at the city scale and vehicle localization to improve online

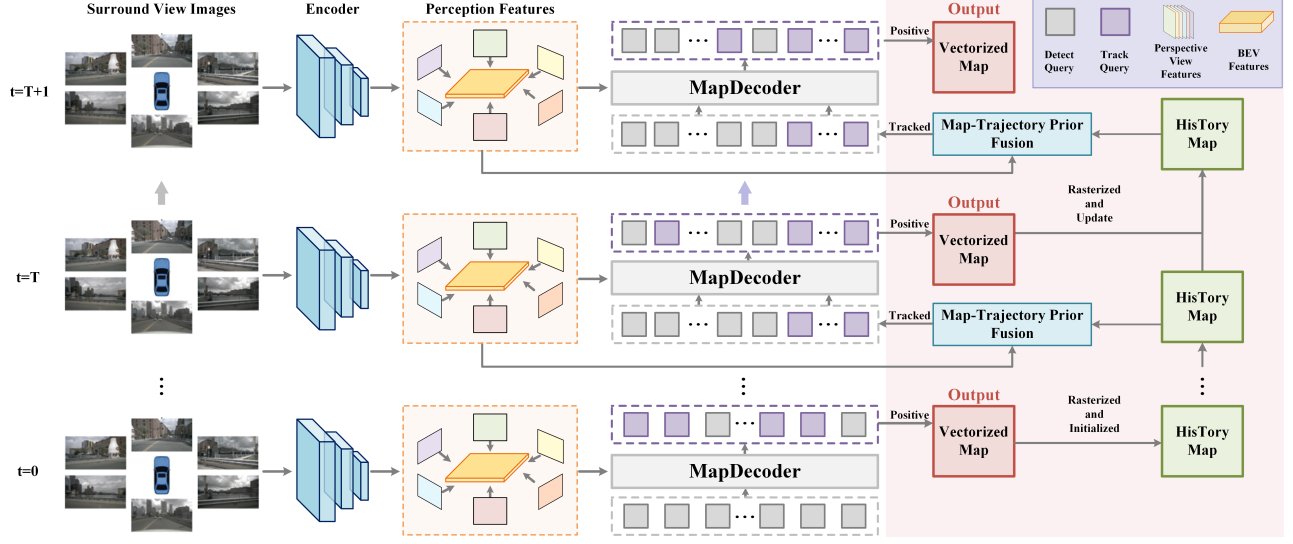


Figure 3. **The architecture pipeline of the HisTrackMap.** Initialization at timestamp 0 and tracking at T and T+1 are illustrated. Track queries associate map elements and construct temporal relationships through the history maps under the tracking paradigm.

vectorized map perception.

**Map Perception with Temporal Framework.** Temporal information is crucial, particularly in complex scenarios with long distances and occlusions, and has been a consistent focus in 3D object detection [6, 8, 16, 28]. StreamMapNet [37] is the first temporal map construction framework. It employs multi-point attention, enabling the construction of large-scale local HD map with high stability. SQD-MapNet [29] introduces the Stream Query Denoising (SQD) strategy for temporal modeling. GlobalMapNet [27] attempts to perform evaluations from a global perspective and proposes Map NMS to obtain a clean global map. MapTracker [3] presents a vector HD-mapping algorithm that formulates the mapping as a tracking task and leverages latent memory to ensure temporally consistent constructions.

**Evaluation Metrics.** MapVR [39] and MGMap [17] evaluate rasterized results using IoU (Intersection over Union) metric. In contrast, MapTR [13, 14] emphasizes point-to-point correspondence and employs Chamfer Distance to calculate average precision. However, these metrics are primarily effective for evaluating instantaneous performance. Since map perception in practice requires evaluation over continuous sequences, these metrics struggle to measure temporal consistency effectively. To address this limitation, MapTracker [3] introduces the consistency-aware metric (C-mAP), which aims to penalize mismatches in perception results based on the alignment of corresponding instances across frames.

### 3. HisTrackMap

#### 3.1. Overview Architecture

Fig. 3 illustrates the framework of the proposed HisTrackMap, built on a tracking paradigm [3, 38]. The encoder extracts perception features (BEV feature  $\mathbf{F}_{bev}$  and PV feature  $\mathbf{F}_{pv}$ ) from surrounding-view images to localize spatial structures. The input detection query  $\mathbf{Q} \in \mathbb{R}^{N_q \times C}$  is updated through MapDecoder to produce the coordinates  $\mathbf{P} \in \mathbb{R}^{N_q \times N_p \times 2}$ , categories  $\mathbf{C} \in \mathbb{R}^{N_q \times 3}$  (pedestrian, boundary, divider) and scores  $\mathbf{S} \in \mathbb{R}^{N_q}$ . Here,  $N_q$  denotes the number of detected queries,  $N_p$  represents the number of points of a map instance, and  $C$  is the feature dimension.

After the decoder, the outputted detected queries and propagated track queries are filtered to be positive using a detection threshold  $\tau_{det}$  and a tracking threshold  $\tau_{track}$ . These positive  $N_{track}$  queries  $\mathbf{Q}_{track}$  are propagated to the next frame as new track queries. Queries with confidence below the thresholds are treated as disappeared instances and discarded as negative queries. In summary, map instances will be categorized as newly appeared, consistently tracked, or disappeared, and the corresponding history maps will be initialized, updated with the rasterized map, or removed accordingly. Furthermore, the Map-Trajectory Prior Fusion utilizes the history map to sample corresponding positions on perception features extracted by the encoder, establishing a strong geometric prior for initializing track queries in the new frame and explicitly optimizing the propagation of track queries across temporal sequences.

Section 3.2 introduces the instance-level history maps for maintaining and updating historical map trajectories. Subsequently, Section 3.3 presents the Map-Trajectory Prior Fusion, which provides prior information to enrich

track queries. Finally, Section 3.4 proposes the metrics to address the current insufficiencies in evaluating stability and continuity in real-world autonomous driving scenarios.

### 3.2. Instance-Level History Maps

We first introduce instance-level maps used for storing historical information. The history map is maintained for the tracked instances generated during online prediction to store their trajectory information. During the propagation process, each track query corresponds to a unique map instance and history map, thereby establishing a strong one-to-one relationship.

At the beginning of frame  $t$ ,  $\mathcal{M}$  is a collection of history maps corresponding to a series of track queries, defined as  $\mathcal{M}^t = \{\mathbf{M}_i^t \mid i = 1, 2, \dots, N_{track}^{t-1}\}$ . Here, each  $\mathbf{M}_i^t \in \mathbb{R}^{H \times W}$  indicates the rasterized history map of the  $i$ -th instance among the  $N_{track}^{t-1}$  instances that have been tracked at the previous frame, where  $H$  and  $W$  are equal to the height and width of the BEV feature, respectively.

Subsequently, the perception results at timestamp  $t$  are used to update the history map. For the  $j$ -th instance, if it is identified as a newly born instance (i.e., no corresponding tracking index is found, and its confidence score  $\mathbf{S}_j^t$  exceeds the detect threshold  $\tau_{det}$ ), the rasterization method  $\text{Raster}(\cdot)$  [39] is employed to transform the vectorized map representation  $\mathbf{P}_j^t$  into a rasterized format. The rasterized result is scaled by  $\mathbf{S}_j^t$  to initialize its history map. If the instance has been tracked (i.e., some tracking index is associated, and  $\mathbf{S}_j^t$  exceeds the tracking threshold  $\tau_{track}$ ), the corresponding historical map  $\mathbf{M}_i^{t-1}$  is retrieved based on its tracking index  $i$ . This history map is then temporally decayed using a decay factor  $\lambda$  and updated with the newly rasterized result, yielding the updated history map  $\mathbf{M}_i^t$  as:

$$\mathbf{M}_i^t = \begin{cases} \text{Raster}(\mathbf{P}_j^t) \cdot \mathbf{S}_j^t, & \text{if newborn,} \\ \max(\lambda \cdot \mathbf{M}_i^{t-1}, \text{Raster}(\mathbf{P}_j^t) \cdot \mathbf{S}_j^t), & \text{if tracked.} \end{cases} \quad (1)$$

After completing the update process, the history map  $\mathbf{M}_i^t$  is finalized. At timestamp  $t$ , both the total number of tracked instances  $N_{track}^t$  and the collection of history maps  $\mathcal{M}^t$  are updated accordingly. At timestamp  $t+1$ ,  $\mathcal{M}^t$  is dynamically aligned with the updated ego position to obtain warped history maps  $\mathcal{M}_w^{t+1}$ , thereby enabling initialization for the subsequent timestamp as

$$\mathcal{M}_w^{t+1} = \text{Warp}(\mathcal{M}^t, \mathcal{T}^{t+1}), \quad (2)$$

where  $\mathcal{T}^{t+1}$  denotes a standard  $4 \times 4$  transformation matrix that characterizes the spatial transformation relationship between the coordinate systems of two consecutive frames,  $\text{Warp}(\cdot)$  is the alignment function.

Note that, if the prediction confidence of some track query is below the  $\tau_{track}$ , it indicates that that instance has

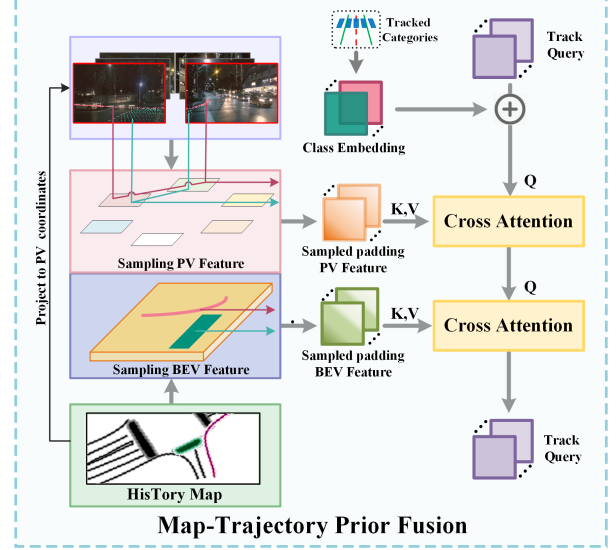


Figure 4. Architecture of Map-Trajectory Prior Fusion.

disappeared or has not been successfully tracked at the current frame. Consequently, it is necessary to remove the corresponding track query and history map  $\mathbf{M}_r$  from  $\mathcal{M}^{t+1}$ , and the total number of tracked instances  $N_{track}^{t+1}$  will be decremented accordingly as:

$$\mathcal{M}^{t+1} = \mathcal{M}_w^{t+1} \setminus \{\mathbf{M}_r\}. \quad (3)$$

Each map instance follows the process of initialization, tracking, and history map updating to achieve the binding of historical trajectory information with the track query, enabling temporal propagation.

### 3.3. Map-Trajectory Prior Fusion

As aforementioned, to address the limitations of implicit temporal propagation in capturing detailed feature transformations during motion, the Map-Trajectory Prior Fusion is designed to integrate historical map trajectory information into track queries, enhancing temporal prior utilization and perceptual consistency. As shown in Fig. 4, the Map-Trajectory Prior Fusion first samples instance features from the history map within the PV and BEV feature spaces. Since the number of instance features varies, padding is applied to align them to a uniform length. These instance-level perception features are then individually integrated into the track queries through cross-attention.

Historical information provides both semantic category and spatial trajectory coordinate data. To enhance the semantic representation of track queries, we define an initial class embedding  $\mathbf{CE}_{init} \in \mathbb{R}^{3 \times C}$ , which encodes previous track categories into a class embedding  $\mathbf{CE} \in \mathbb{R}^{N_{track} \times C}$ . The class embedding is fused with the track query to provide category priors as

$$\mathbf{Q}_{track} = \mathbf{Q}_{track} + \mathbf{CE}. \quad (4)$$



The history map is a fine-grained map with temporal decay. Therefore, we generate the valid pixel mask  $\mathcal{M}_{val}$  by filtering pixels in  $\mathcal{M}$  that exceed the map threshold  $\tau_{map}$ . To enhance the spatial awareness of PV features in 3D space, learnable coordinate embeddings  $\mathbf{PE}_{coords} \in \mathbb{R}^{h \times w \times C}$  are combined with camera embeddings  $\mathbf{PE}_{cam} \in \mathbb{R}^{cams \times C}$  generated via the ego-to-image matrix  $\mathbf{E2I} \in \mathbb{R}^{cams \times 4 \times 4}$ , producing the final PV position embedding  $\mathbf{PE}_{pv} \in \mathbb{R}^{cams \times h \times w \times C}$  as

$$\mathbf{PE}_{pv} = \mathbf{PE}_{cam} + \mathbf{PE}_{coords}, \quad (5)$$

where  $h, w$  are the resolutions of the PV features, and  $cams$  is the number of cameras.

Then, we project  $\mathcal{M}_{val}$  into the perspective view space using the projection function  $\text{Proj}(\cdot)$ . In this space, the PV features  $\mathbf{F}_{pv}$  are combined with the corresponding positional embedding  $\mathbf{PE}_{pv}$  to form enhanced feature representations. Subsequently, the  $\text{SampledPV}(\cdot)$  function is applied to sample from these enhanced features, resulting in the final sampled PV features  $\mathbf{F}_{sampled.pv}$  as

$$\mathbf{F}_{sampled.pv} = \text{SampledPV}(\text{Proj}(\mathcal{M}_{val}, \mathbf{E2I}), \mathbf{F}_{pv} + \mathbf{PE}_{pv}). \quad (6)$$

Similarly, we perform analogous operations in the Bird's-Eye View space. To ensure that the sampled BEV features  $\mathbf{F}_{sampled.bev}$  incorporate positional information, we introduce a sinusoidal position embedding  $\mathbf{PE}_{bev} \in \mathbb{R}^{H \times W \times C}$ . Then, we utilize  $\mathcal{M}_{val}$  to sample BEV feature  $\mathbf{F}_{bev}$  through the  $\text{SampledBEV}(\cdot)$  function as

$$\mathbf{F}_{sampled.bev} = \text{SampledBEV}(\mathcal{M}_{val}, \mathbf{F}_{bev} + \mathbf{PE}_{bev}). \quad (7)$$

Next, the PV and BEV features corresponding to each instance, including the historical map trajectories, have been obtained. The track queries, along with their associated sampled features  $\mathbf{F}_{sampled.bev}$  and  $\mathbf{F}_{sampled.pv}$ , are then utilized within a cross-attention  $\text{CA}(\cdot)$  to finalize the initialization of the track queries for the current timestamp:

$$\begin{aligned} \mathbf{Q}_{track} &= \text{CA}(\mathbf{Q}_{track}, \mathbf{F}_{sampled.pv}), \\ \mathbf{Q}_{track} &= \text{CA}(\mathbf{Q}_{track}, \mathbf{F}_{sampled.bev}). \end{aligned} \quad (8)$$

Finally, we explicitly leverage historical trajectories to provide precise priors for track queries, avoiding redundant auxiliary supervision and inaccurate temporal transformations in implicit propagation. Notably, since the valid pixels for each instance vary, we pad the features and apply a padding mask to ensure that each track query focuses on its corresponding positions.

### 3.4. Global Geometric HD Mapping Evaluation

Current map construction metrics have the following limitations: (1) Single-frame mAP [14] does not adequately

---

#### Algorithm 1 Global\_Instance\_Match

---

**Require:** Distance cost matrix  $\mathbf{CM}$ ,  
average confidence scores  $\mathbf{AS}$ ,  
distance threshold  $\tau_{dis} = \{0.25, 0.5, 0.75, 1.0\}$ ,  
valid threshold  $\tau_{valid} = 2$

**Ensure:** True positives  $\mathbf{TP}$ , false positives  $\mathbf{FP}$

```

1:  $\mathbf{TP} \leftarrow \text{zeros}(\mathbf{CM.shape}[0])$ 
2:  $\mathbf{FP} \leftarrow \text{zeros}(\mathbf{CM.shape}[0])$ 
3:  $\text{gt\_covered} \leftarrow \text{zeros}(\mathbf{CM.shape}[1], \text{dtype} = \text{bool})$ 
4: for  $i$  in  $\text{argsort}(-\mathbf{AS})$  do
5:   if  $\mathbf{CM}[i].\text{min}() \leq \tau_{dis}$  then
6:     for  $j$  in  $\mathbf{CM.shape}[1]$  do
7:       if  $\mathbf{CM}[i][j] \leq \tau_{dis}$  and  $\text{gt\_covered}[j] == \text{False}$  then
8:          $\text{gt\_covered}[j] \leftarrow \text{True}$ 
9:          $\mathbf{TP}[i] \leftarrow \mathbf{TP}[i] + 1$  // Match multiple ground truth instances
10:      end if
11:    end for
12:  else if  $\mathbf{CM}[i].\text{min}() > \tau_{dis} + \tau_{valid}$  then
13:     $\mathbf{FP}[i] \leftarrow 0$  // Invalid FP
14:  else if  $\mathbf{CM}[i].\text{min}() \leq \tau_{dis} + \tau_{valid}$  then
15:     $\mathbf{FP}[i] \leftarrow 1$  // Valid FP
16:  end if
17: end for
```

---

capture the overall quality of a map, as it emphasizes local and instantaneous evaluations while neglecting the assessment of continuity and consistency. (2) consistency-aware C-mAP [3] indirectly addresses consistency but does not explicitly evaluate map completeness. To address these, we propose a global geometric-aware metric (G-mAP) that evaluates construction quality from a global perspective.

First, the vectorized ground truth elements  $\mathbf{P}_{local}^{gt}$  from  $N_{seq}$  single frames of a sequence segment are projected into a global coordinate system and rasterized to produce a complete global map containing all map instances  $\mathbf{P}_{global}^{gt}$  as

$$\mathbf{P}_{global}^{gt} = \text{RasterGlobal}(\{\mathbf{P}_{local}^{gt}\}_{i=1}^{N_{seq}}), \quad (9)$$

where  $\text{RasterGlobal}(\cdot)$  denotes the process of transforming local coordinates into the global coordinate system and performing rasterization.

To address truncation issues of polygons (e.g., pedestrians) during vehicle motion, it is more effective to evaluate them using IoU metrics [39]. Thus, we adopt the rasterization-based mAP to evaluate closed pedestrian masks with  $AP_{polygon}$ . For polyline categories, we use the Merge function [3]  $\text{Merge}(\cdot)$  to combine the tracking results  $\mathbf{P}_{local}^{pred}$  from each frame, obtaining a globally complete instance vector  $\mathbf{P}_{global}^{pred}$  as

$$\mathbf{P}_{global}^{pred} = \text{Merge}(\{\mathbf{P}_{local}^{pred}\}_{i=1}^{N_{seq}}). \quad (10)$$

To obtain the vector representation of the entire instance, the ground truth mask of the corresponding instance is utilized to extract discrete points via Farthest Point Sampling [24], enabling the fitting of the complete polyline. Subsequently, the  $AP_{polyline}$  is calculated using the Chamfer Distance metric [14].

G-mAP leverages the strengths of both rasterized and vectorized representations. It consists of two components: rasterization-based mAP for polygons (e.g., pedestrian) and vectorization-based mAP for polylines (e.g., divider and boundary). By averaging the results across the three categories, G-mAP achieves a comprehensive evaluation from a global geometric perspective.

The `Global_Instance_Match` function is used to obtain false positives (FP) and true positives (TP) under the Chamfer Distance metric. We construct a distance cost matrix  $\mathbf{CM} \in \mathbb{R}^{N_{pred} \times N_{gt}}$  using  $N_{pred}$  predictions and  $N_{gt}$  ground truths, which represents the average distance between the predicted point coordinates and the ground truth for each instance. Additionally, we compute the average confidence scores  $\mathbf{AS} \in \mathbb{R}^{N_{pred}}$  for each instance and define a distance threshold  $\tau_{dis}$  to evaluate the vectorization-based mAP across different thresholds. It is worth noting that we have optimized the evaluation algorithm due to the unique characteristics of the global perspective. As shown in Algorithm 1, to prevent overlooking shorter instances that have been accurately identified, our algorithm permits predicted instances to correspond to multiple shorter ground truth instances in the global perspective by incrementing the true positive (TP) count. In addition, there are instances in practice that have been perceived but not labelled. To address this issue, we use a validity threshold  $\tau_{valid}$  to constrain the counting of false positives (FP).

## 4. Experiments

### 4.1. Experimental Settings

**Dataset.** We evaluate HisTrackMap on two popular autonomous driving datasets: nuScenes and Argoverse 2. The nuScenes [1] dataset contains 1,000 scenes, each spanning 20 seconds, with data from six synchronized RGB cameras and detailed pose information. The Argoverse 2 dataset [30] includes 1,000 sequences with high-resolution images from seven ring cameras, two stereo cameras, LiDAR point clouds, and map-aligned 6-DoF pose data. Experiments were conducted on both the old [14] and new [37] dataset splits for comprehensive evaluation.

**Metrics.** Following previous work [3, 13, 14, 35, 37], we adopt mean Average Precision (mAP) as the primary evaluation metric. Evaluation thresholds are set at 0.5m, 1.0m, and 1.5m.  $AP_{ped}$ ,  $AP_{div}$ , and  $AP_{bou}$  represent average precision for pedestrians, dividers, and boundaries, respectively. In addition, we employ consistency-aware metric (C-

mAP) [3] and further introduce a novel global geometric-aware augmented metric (G-mAP), as detailed in Sec. 3.4.

**Implementation Details.** Our framework builds on MapTracker [3], which serves as the primary baseline. We removed the Motion MLP and the auxiliary transformation loss used for its supervision while keeping other loss functions consistent with MapTracker. Training on the nuScenes [1] dataset was conducted on 8 NVIDIA RTX A100 GPUs for 72 epochs across three stages (18, 6, and 48 epochs). Similarly, we trained on the Argoverse2 [30] dataset for 35 epochs (12, 3, and 20 epochs) to align with MapTracker. Additionally, to ensure alignment with methods such as MapTR [14, 35, 41], we evaluated a shorter 24-epoch training configuration on both datasets. To address inaccuracies in the PV projection caused by the dataset’s missing Z-axis coordinates, we introduced a complete Map-Trajectory Prior Fusion in Stage 2 to accelerate model convergence. In Stage 3, we exclusively adopted a single BEV Prior to further enhancing model performance. The hyperparameters are configured as  $N_q = 100$ ,  $N_p = 20$ ,  $C = 512$ ,  $\tau_{det} = 0.4$ ,  $\tau_{track} = 0.5$ ,  $\tau_{map} = 0.5$ ,  $\lambda = 0.95$ .

### 4.2. Comparison with SOTA Method

**Comparison on nuScenes.** As shown in Table 1, we compare HisTrackMap with state-of-the-art methods. HisTrackMap demonstrates superior performance at 24 epochs, achieving 73.8 mAP, outperforming MapTracker, which achieves 71.9 mAP, by +1.9 mAP. In addition, HisTrackMap achieves 64.7 C-mAP and 48.5 G-mAP, outperforming MapTracker by +1.3 C-mAP and +1.2 G-mAP, respectively. In the 72-epoch experiment, HisTrackMap achieved 76.6 mAP, 68.7 C-mAP, and 50.2 G-mAP respectively. Furthermore, recent methods like Mask2Map and MGMap use single-frame frameworks with limited temporal modeling, while HisTrackMap outperforms them in all metrics. Notably, by removing transformation loss supervision of Motion MLP, HisTrackMap achieves about 20% faster training than MapTracker. During inference, HisTrackMap runs at 10.3 FPS, slightly slower than MapTracker’s 10.9 FPS due to feature sampling overhead, which could be optimized with parallel acceleration in practical applications. In summary, HisTrackMap improves performance and remains practical for real-time autonomous driving applications.

**Comparison on Argoverse 2.** The results on the Argoverse 2 dataset, as presented in Table 2, further validate the effectiveness of HisTrackMap. In the 24-epoch experiment, HisTrackMap achieves a notable mAP improvement of +8.5 over HRMapNet and +9.4 over MapTRv2. Additionally, HisTrackMap surpasses MapTracker with +1.2 mAP, +3.5 C-mAP, and +0.8 G-mAP at 24 epochs, and +0.9 mAP, +1.2 C-mAP, and +0.6 G-mAP at 35 epochs. Note that due to the different sampling intervals of HisTrackMap and Map-

| Method                                 | Epoch | $AP_{ped}$  | $AP_{div}$  | $AP_{bou}$  | mAP         | C-mAP       | G-mAP       | FPS  |
|--|-------|-------------|-------------|-------------|-------------|-------------|-------------|------|
| MapTRv2 [14] [IJCV2024]                | 24    | 59.8        | 62.4        | 62.4        | 61.4        | 41.7        | 33.9        | 14.1 |
| StreamMapNet [29] [WACV2024]           | 24    | 61.9        | 66.3        | 62.1        | 63.4        | 38.4        | 34.3        | 13.1 |
| HRMapNet [41] [ECCV2024]               | 24    | 65.8        | 67.4        | 68.5        | 67.3        | 49.2        | 39.7        | 10.3 |
| MGMap [17] [CVPR2024]                  | 24    | 61.8        | 65.0        | 67.5        | 64.8        | 43.5        | 39.1        | 13.4 |
| MGMapNet [35] [ICLR2025]               | 24    | 64.7        | 66.1        | 69.4        | 66.8        | 45.4        | 37.5        | 11.7 |
| Mask2Map [4] [ECCV2024]                | 24    | 70.6        | 71.3        | <b>72.9</b> | 71.6        | 55.8        | 44.5        | 9.2  |
| MapTracker [3] <sup>†</sup> [ECCV2024] | 24    | 75.3        | 69.2        | 71.2        | 71.9        | 63.4        | 47.3        | 10.9 |
| <b>HisTrackMap (Ours)</b>              | 24    | <b>76.9</b> | <b>72.7</b> | 71.9        | <b>73.8</b> | <b>64.7</b> | <b>48.5</b> | 10.3 |
| HRMapNet [41] [ECCV2024]               | 110   | 72.0        | 72.9        | 75.8        | 73.6        | 61.4        | 47.9        | 10.3 |
| Mask2Map [4] [ECCV2024]                | 110   | 73.6        | 73.1        | <b>77.3</b> | 74.6        | 60.3        | 48.8        | 9.2  |
| MapTracker [3] [ECCV2024]              | 72    | <b>80.0</b> | 74.1        | 74.1        | 76.1        | <b>69.1</b> | 49.4        | 10.9 |
| <b>HisTrackMap (Ours)</b>              | 72    | 79.8        | <b>74.5</b> | 75.4        | <b>76.6</b> | 68.7        | <b>50.2</b> | 10.3 |

Table 1. Comparison with SOTA methods on the nuScenes validation set. <sup>†</sup> indicates the version reproduced.

| Method                                 | epoch | $AP_{ped}$  | $AP_{div}$  | $AP_{bou}$  | mAP         | C-mAP       | G-mAP       |
|--|-------|-------------|-------------|-------------|-------------|-------------|-------------|
| MapTRv2 [14] [IJCV2024]                | 24    | 62.9        | 72.1        | 67.1        | 67.4        | —           | —           |
| HRMapNet [41] [ECCV2024]               | 30    | 65.1        | 71.4        | 68.6        | 68.3        | —           | —           |
| HIMap [43] [CVPR2024]                  | 24    | 72.4        | 72.4        | 73.2        | 72.7        | —           | —           |
| MGMapNet [35] [ICLR2025]               | 24    | 71.3        | 76.0        | 73.1        | 73.6        | —           | —           |
| MapTracker [3] <sup>†</sup> [ECCV2024] | 24    | 75.0        | 78.7        | 73.1        | 75.6        | 63.1        | 47.4        |
| <b>HisTrackMap (Ours)</b>              | 24    | <b>77.4</b> | <b>78.9</b> | <b>74.1</b> | <b>76.8</b> | <b>66.6</b> | <b>48.2</b> |
| MapTracker [3] [ECCV2024]              | 35    | 76.9        | 79.9        | 73.6        | 76.8        | 68.3        | 48.0        |
| <b>HisTrackMap (Ours)</b>              | 35    | <b>78.8</b> | <b>80.1</b> | <b>74.0</b> | <b>77.7</b> | <b>69.5</b> | <b>48.6</b> |

Table 2. Comparison with SOTA methods on the Argoverse2 validation set. The ‘—’ symbol indicates that no results are provided.

Tracker on the Argoverse 2 dataset compared to the other methods, we can only evaluate the mAP metrics.

| Dataset          | Method      | mAP  | C-mAP | G-mAP |
|------------------|-------------|------|-------|-------|
| nuScenes         | MapTracker  | 40.3 | 32.5  | 28.0  |
|                  | HisTrackMap | 41.5 | 32.8  | 28.5  |
| Argoverse2       | MapTracker  | 70.3 | 61.3  | 48.3  |
|                  | HisTrackMap | 71.4 | 62.7  | 49.2  |
| Unified nuScenes | MapTracker  | 43.5 | 34.0  | 29.9  |
|                  | HisTrackMap | 44.5 | 35.1  | 31.2  |

Table 3. Comparisons on non-overlapping datasets.

**Comparison on non-overlapping datasets.** The nuScenes and Argoverse 2 datasets exhibit geographical overlaps [15]. StreamMapNet [29] proposes a non-overlapping dataset split for them. The experimental results are shown in Table 3. Our method surpasses MapTracker, achieving improvements of +1.2 mAP, +0.3 C-mAP, and +0.5 G-mAP on nuScenes, and +1.1 mAP, +1.4 C-mAP, and +0.9 G-mAP on Argoverse 2. We conducted cross-dataset experiments to demonstrate further the superior generalization of HisTrackMap. The encoder and decoder were initialized with weights from nuScenes and Argoverse 2 respectively, and finetuned for 12 epochs on the nuScenes

newsplit before testing. HisTrackMap achieved 44.5 mAP, 35.1 C-mAP, and 31.2 G-mAP, demonstrating superior generalization performance over MapTracker.

### 4.3. Quantitative Evaluations

Fig. 5 presents a qualitative comparison between HisTrackMap and other methods on nuScenes dataset. We utilized the integration [3] of per-frame vectorized HD maps into a global vectorized HD map for better visualization. The rectangular regions highlight instances where our proposed model exhibits superior perception performance. The orange markings indicate that HisTrackMap accurately identified the two separate boundaries at the turning, whereas MapTracker failed to distinguish them. The blue markings highlight that HisTrackMap achieved continuous and consistent tracking through a complex intersection, whereas MapTracker lost the polyline. The green markings indicate that HisTrackMap fully detected the boundary, while MapTracker captured only the first half. In this green example, all models detected a divider that was not actually annotated, emphasizing the necessity of optimizing false positive (FP) counting in G-mAP. Furthermore, although single-frame MapTRv2 can partially perceive results, the integrated results lack sufficient stability and fail to maintain consistent perception. In general, HisTrackMap

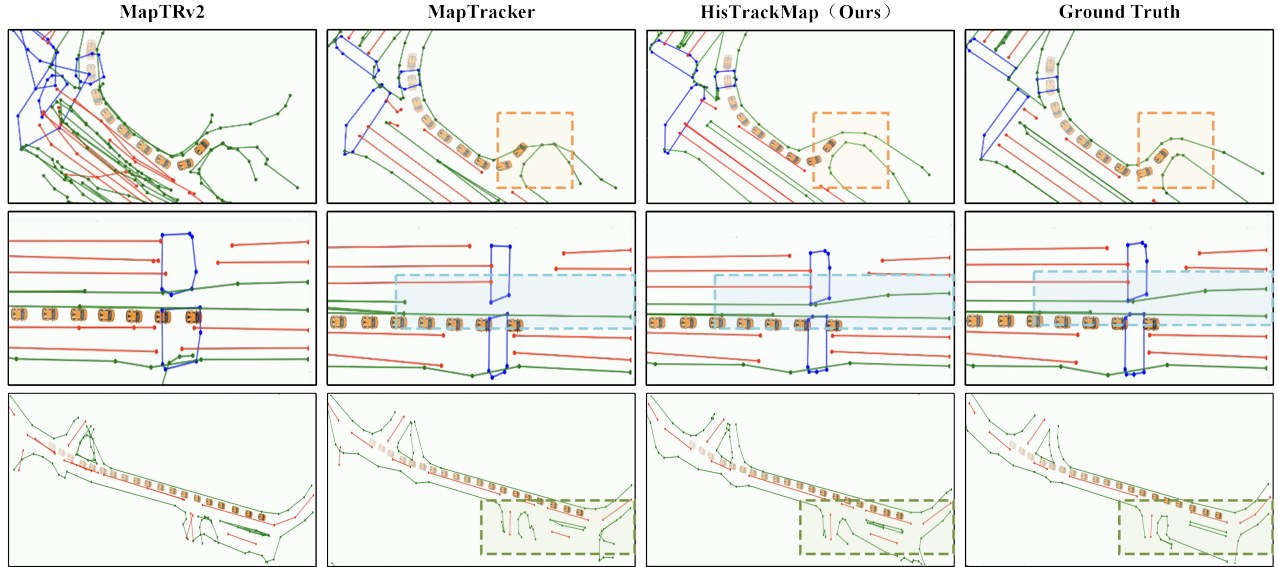


Figure 5. Qualitative visualization on nuScenes val set.

delivers more accurate and cleaner results, demonstrating superior performance in terms of overall quality and temporal consistency.

#### 4.4. Ablation and Robustness Studies

The proposed Map-Trajectory Prior Fusion consists of three main components: Class Embedding, PV Prior, and BEV Prior. To evaluate the contributions of each component, we conducted an ablation study on the nuScenes dataset, with the results presented in Tab. 4. The experiment without Map-Trajectory Prior Fusion is used as the baseline. There are several observations from the results. First, introducing Class Embedding improved mAP by 0.7, demonstrating the effectiveness of semantic category priors. Second, incorporating PV Prior and BEV Prior based on Class Embedding further improves mAP from 72.3 to 72.9 and 73.3, respectively. This reveals that it is beneficial to utilize geometric trajectory information to enhance track queries. Third, with the complete Map-Trajectory Prior Fusion, the model achieved the highest 73.8 mAP, highlighting the significance of history map based trajectory priors in effectively leveraging temporal-spatial information to enhance perception performance.

The update of the history map primarily relies on the vehicle’s motion pose parameters. To evaluate the robustness of HisTrackMap to localization errors, we conducted additional experiments on the nuScenes dataset, as detailed in Tab. 5. Random noise was introduced to the translation and rotation of the extrinsic matrix to disrupt the history map update. The results show that the model achieves 73.0 mAP under noise levels of 0.2 m and 0.02 rad and 73.4 mAP under real-world noise levels (0.1 m, 0.01 rad), maintaining a clear advantage. The experimental results continue to out-

| Map-Trajectory Prior Fusion |          |           | mAP  |
|-----------------------------|----------|-----------|------|
| Class Embed.                | PV Prior | BEV Prior |      |
| —                           | —        | —         | 71.6 |
| ✓                           | —        | —         | 72.3 |
| ✓                           | ✓        | —         | 72.9 |
| ✓                           | —        | ✓         | 73.3 |
| ✓                           | ✓        | ✓         | 73.8 |

Table 4. Ablation study of the Map-Trajectory Prior Fusion.

|                  |      | $\sigma_t$ (m) |      |      |
|------------------|------|----------------|------|------|
|                  |      | 0              | 0.1  | 0.2  |
| $\sigma_r$ (rad) | 0    | 73.8           | 73.6 | 73.5 |
|                  | 0.01 | 73.5           | 73.4 | 73.1 |
|                  | 0.02 | 73.3           | 73.2 | 73.0 |

Table 5. Robustness study with different localization errors.

perform most previous single-frame models, demonstrating the practical effectiveness of HisTrackMap.

## 5. Conclusion

In this work, we introduce a novel method for end-to-end vectorized HD map construction via tracking history maps, enabling more robust and efficient temporal association modeling. Specifically, the history map is systematically constructed and updated based on past perception results, thereby minimizing redundant computations. We introduce the Map-Trajectory Prior Fusion method, which integrates historical map data with current perception features to improve the precision of frame-to-frame transfor-



mations. Additionally, we propose a global geometric HD mapping evaluation framework that focuses on assessing overall map construction quality. This evaluation is vital for both autonomous driving systems and map data collection processes. In the future, it is desired to extend the current work by exploring a more robust, reliable, and adaptive perception system considering the existence of vehicle localization errors.

## References

- [1] Holger Caesar, Varun Bankiti, Alex H Lang, Sourabh Vora, Venice Erin Liong, Qiang Xu, Anush Krishnan, Yu Pan, Giancarlo Baldan, and Oscar Beijbom. nuScenes: a multi-modal dataset for autonomous driving. In *Proceedings of the IEEE/CVF conference on computer vision and pattern recognition*, pages 11621–11631, 2020. 2, 6
- [2] Nicolas Carion, Francisco Massa, Gabriel Synnaeve, Nicolas Usunier, Alexander Kirillov, and Sergey Zagoruyko. End-to-end object detection with transformers. In *European conference on computer vision*, pages 213–229. Springer, 2020. 1
- [3] Jiacheng Chen, Yuefan Wu, Jiaqi Tan, Hang Ma, and Yasutaka Furukawa. MapTracker: tracking with strided memory fusion for consistent vector HD mapping. In *European Conference on Computer Vision*, pages 90–107. Springer, 2025. 1, 3, 5, 6, 7
- [4] Sehwan Choi, Jungho Kim, Hongjae Shin, and Jun Won Choi. Mask2Map: vectorized HD map construction using bird’s eye view segmentation masks. *arXiv preprint arXiv:2407.13517*, 2, 2024. 2, 7
- [5] Wenjie Ding, Limeng Qiao, Xi Qiu, and Chi Zhang. PivotNet: vectorized pivot learning for end-to-end HD map construction. In *Proceedings of the IEEE/CVF International Conference on Computer Vision*, pages 3672–3682, 2023. 2
- [6] Chunrui Han, Jinrong Yang, Jianjian Sun, Zheng Ge, Runpei Dong, Hongyu Zhou, Weixin Mao, Yuang Peng, and Xiangyu Zhang. Exploring recurrent long-term temporal fusion for multi-view 3D perception. *IEEE Robotics and Automation Letters*, 2024. 3
- [7] Anthony Hu, Zak Murez, Nikhil Mohan, Sofia Dudas, Jeffrey Hawke, Vijay Badrinarayanan, Roberto Cipolla, and Alex Kendall. FIERY: future instance prediction in bird’s-eye view from surround monocular cameras. In *Proceedings of the IEEE/CVF International Conference on Computer Vision*, pages 15273–15282, 2021. 1
- [8] Junjie Huang and Guan Huang. BEVDet4D: exploit temporal cues in multi-camera 3D object detection. *arXiv preprint arXiv:2203.17054*, 2022. 3
- [9] Zhou Jiang, Zhenxin Zhu, Pengfei Li, Huan-ang Gao, Tianyuan Yuan, Yongliang Shi, Hang Zhao, and Hao Zhao. P-MapNet: far-seeing map generator enhanced by both SDMap and HDMMap priors. *arXiv preprint arXiv:2403.10521*, 2024. 2
- [10] Qi Li, Yue Wang, Yilun Wang, and Hang Zhao. HDMMapNet: an online HD map construction and evaluation framework. In *2022 International Conference on Robotics and Automation (ICRA)*, pages 4628–4634. IEEE, 2022. 1
- [11] Tengpeng Li, Hanli Wang, Xianfei Li, Wenlong Liao, Tao He, and Pai Peng. Generative planning with 3d-vision language pre-training for end-to-end autonomous driving. *arXiv preprint arXiv:2501.08861*, 2025. 1
- [12] Zhiqi Li, Wenhai Wang, Hongyang Li, Enze Xie, Chonghao Sima, Tong Lu, Qiao Yu, and Jifeng Dai. BEVFormer: learning bird’s-eye-view representation from lidar-camera via spatiotemporal transformers. *IEEE Transactions on Pattern Analysis and Machine Intelligence*, 2024. 2
- [13] Bencheng Liao, Shaoyu Chen, Xinggang Wang, Tianheng Cheng, Qian Zhang, Wenyu Liu, and Chang Huang. MapTR: structured modeling and learning for online vectorized HD map construction. *arXiv preprint arXiv:2208.14437*, 2022. 1, 2, 3, 6
- [14] Bencheng Liao, Shaoyu Chen, Yunchi Zhang, Bo Jiang, Qian Zhang, Wenyu Liu, Chang Huang, and Xinggang Wang. MapTRv2: an end-to-end framework for online vectorized HD map construction. *arXiv preprint arXiv:2308.05736*, 2023. 1, 2, 3, 5, 6, 7
- [15] Adam Lilja, Junsheng Fu, Erik Stenborg, and Lars Hammarstrand. Localization is all you evaluate: data leakage in online mapping datasets and how to fix it. In *Proceedings of the IEEE/CVF Conference on Computer Vision and Pattern Recognition*, pages 22150–22159, 2024. 7
- [16] Xuewu Lin, Tianwei Lin, Zixiang Pei, Lichao Huang, and Zhizhong Su. Sparse4D v2: recurrent temporal fusion with sparse model. *arXiv preprint arXiv:2305.14018*, 2023. 3
- [17] Xiaolu Liu, Song Wang, Wentong Li, Ruizi Yang, Junbo Chen, and Jianke Zhu. MGMap: mask-guided learning for online vectorized HD map construction. In *Proceedings of the IEEE/CVF Conference on Computer Vision and Pattern Recognition*, pages 14812–14821, 2024. 3, 7
- [18] Yingfei Liu, Tiancai Wang, Xiangyu Zhang, and Jian Sun. PETR: position embedding transformation for multi-view 3D object detection. In *European conference on computer vision*, pages 531–548. Springer, 2022. 2
- [19] Yingfei Liu, Junjie Yan, Fan Jia, Shuailin Li, Aqi Gao, Tiancai Wang, and Xiangyu Zhang. PETR v2: a unified framework for 3D perception from multi-camera images. In *Proceedings of the IEEE/CVF International Conference on Computer Vision*, pages 3262–3272, 2023.
- [20] Yicheng Liu, Tianyuan Yuan, Yue Wang, Yilun Wang, and Hang Zhao. VectorMapNet: end-to-end vectorized HD map learning. In *International Conference on Machine Learning*, pages 22352–22369. PMLR, 2023. 2
- [21] Katie Z Luo, Xinhua Weng, Yan Wang, Shuang Wu, Jie Li, Kilian Q Weinberger, Yue Wang, and Marco Pavone. Augmenting lane perception and topology understanding with standard definition navigation maps. In *2024 IEEE International Conference on Robotics and Automation (ICRA)*, pages 4029–4035. IEEE, 2024. 2
- [22] Jonah Philion and Sanja Fidler. Lift, splat, shoot: encoding images from arbitrary camera rigs by implicitly unprojecting to 3D. In *Computer Vision—ECCV 2020: 16th European Conference, Glasgow, UK, August 23–28, 2020, Proceedings, Part XIV 16*, pages 194–210. Springer, 2020. 2
- [23] Aditya Prakash, Kashyap Chitta, and Andreas Geiger. Multi-modal fusion transformer for end-to-end autonomous driv-

- ing. In *Proceedings of the IEEE/CVF conference on computer vision and pattern recognition*, pages 7077–7087, 2021. 1
- [24] Charles Ruizhongtai Qi, Li Yi, Hao Su, and Leonidas J Guibas. PointNet++: deep hierarchical feature learning on point sets in a metric space. *Advances in neural information processing systems*, 30, 2017. 6
- [25] Tixiao Shan and Brendan Englot. LeGO-LOAM: lightweight and ground-optimized lidar odometry and mapping on variable terrain. In *2018 IEEE/RSJ International Conference on Intelligent Robots and Systems (IROS)*, pages 4758–4765. IEEE, 2018. 1
- [26] Tixiao Shan, Brendan Englot, Drew Meyers, Wei Wang, Carlo Ratti, and Daniela Rus. LIO-SAM: tightly-coupled lidar inertial odometry via smoothing and mapping. In *2020 IEEE/RSJ international conference on intelligent robots and systems (IROS)*, pages 5135–5142. IEEE, 2020. 1
- [27] Anqi Shi, Yuze Cai, Xiangyu Chen, Jian Pu, Zeyu Fu, and Hong Lu. GlobalMapNet: An online framework for vectorized global hd map construction. *arXiv preprint arXiv:2409.10063*, 2024. 3
- [28] Shihao Wang, Yingfei Liu, Tiancai Wang, Ying Li, and Xiangyu Zhang. Exploring object-centric temporal modeling for efficient multi-view 3D object detection. In *Proceedings of the IEEE/CVF international conference on computer vision*, pages 3621–3631, 2023. 3
- [29] Shuo Wang, Fan Jia, Yingfei Liu, Yucheng Zhao, Zehui Chen, Tiancai Wang, Chi Zhang, Xiangyu Zhang, and Feng Zhao. Stream query denoising for vectorized HD map construction. *arXiv preprint arXiv:2401.09112*, 2024. 1, 3, 7
- [30] Benjamin Wilson, William Qi, Tanmay Agarwal, John Lambert, Jagjeet Singh, Siddhesh Khandelwal, Bowen Pan, Ratnesh Kumar, Andrew Hartnett, Jhony Kaesemodel Pontes, et al. Argoverse 2: next generation datasets for self-driving perception and forecasting. *arXiv preprint arXiv:2301.00493*, 2023. 2, 6
- [31] Yi Xiao, Felipe Codevilla, Akhil Gurram, Onay Urfalioglu, and Antonio M López. Multimodal end-to-end autonomous driving. *IEEE Transactions on Intelligent Transportation Systems*, 23(1):537–547, 2020. 1
- [32] Xuan Xiong, Yicheng Liu, Tianyuan Yuan, Yue Wang, Yilun Wang, and Hang Zhao. Neural map prior for autonomous driving. In *Proceedings of the IEEE/CVF Conference on Computer Vision and Pattern Recognition*, pages 17535–17544, 2023.
- [33] Zhenhua Xu, Yujia Zhang, Enze Xie, Zhen Zhao, Yong Guo, Kwan-Yee K Wong, Zhenguo Li, and Hengshuang Zhao. DriveGPT4: interpretable end-to-end autonomous driving via large language model. *IEEE Robotics and Automation Letters*, 2024. 1
- [34] Chenyu Yang, Yuntao Chen, Hao Tian, Chenxin Tao, Xizhou Zhu, Zhaoxiang Zhang, Gao Huang, Hongyang Li, Yu Qiao, Lewei Lu, et al. BEVFormer v2: adapting modern image backbones to bird’s-eye-view recognition via perspective supervision. In *Proceedings of the IEEE/CVF Conference on Computer Vision and Pattern Recognition*, pages 17830–17839, 2023. 2
- [35] Jing Yang, Minyue Jiang, Sen Yang, Xiao Tan, Yingying Li, Errui Ding, Hanli Wang, and Jingdong Wang. MGMapNet: multi-granularity representation learning for end-to-end vectorized HD map construction. *arXiv preprint arXiv:2410.07733*, 2024. 2, 6, 7
- [36] Sen Yang, Minyue Jiang, Ziwei Fan, Xiaolu Xie, Xiao Tan, Yingying Li, Errui Ding, Liang Wang, and Jingdong Wang. TopoSD: topology-enhanced lane segment perception with SDMap prior. *arXiv preprint arXiv:2411.14751*, 2024. 2
- [37] Tianyuan Yuan, Yicheng Liu, Yue Wang, Yilun Wang, and Hang Zhao. StreamMapNet: streaming mapping network for vectorized online HD map construction. In *Proceedings of the IEEE/CVF Winter Conference on Applications of Computer Vision*, pages 7356–7365, 2024. 1, 2, 3, 6
- [38] Fangao Zeng, Bin Dong, Yuang Zhang, Tiancai Wang, Xiangyu Zhang, and Yichen Wei. MOTR: end-to-end multiple-object tracking with transformer. In *European Conference on Computer Vision*, pages 659–675. Springer, 2022. 3
- [39] Gongjie Zhang, Jiahao Lin, Shuang Wu, Zhipeng Luo, Yang Xue, Shijian Lu, Zuoguan Wang, et al. Online map vectorization for autonomous driving: a rasterization perspective. *Advances in Neural Information Processing Systems*, 36, 2024. 3, 4, 5
- [40] Ji Zhang, Sanjiv Singh, et al. LOAM: lidar odometry and mapping in real-time. In *Robotics: Science and systems*, pages 1–9. Berkeley, CA, 2014. 1
- [41] Xiaoyu Zhang, Guangwei Liu, Zihao Liu, Ningyi Xu, Yunhui Liu, and Ji Zhao. Enhancing vectorized map perception with historical rasterized maps. In *European Conference on Computer Vision*, pages 422–439. Springer, 2025. 2, 6, 7
- [42] Zhixin Zhang, Yiyuan Zhang, Xiaohan Ding, Fusheng Jin, and Xiangyu Yue. Online vectorized HD map construction using geometry. In *European Conference on Computer Vision*, pages 73–90. Springer, 2025. 2
- [43] Yi Zhou, Hui Zhang, Jiaqian Yu, Yifan Yang, Sangil Jung, Seung-In Park, and ByungIn Yoo. HIMap: hybrid representation learning for end-to-end vectorized HD map construction. In *Proceedings of the IEEE/CVF Conference on Computer Vision and Pattern Recognition*, pages 15396–15406, 2024. 7